Nigerian Journal of Theoretical and Environmental Physics (NJTEP)
ISSN Print: 3026-9601
ISSN Online: 1597-9849
DOI: https://doi.org/10.62292/njtep.v4i2.2026.158
Volume 4(2), June 2026

Multivariate Statistical Evaluation and Comparative Risk Ranking of Natural Radionuclides in Nigerian Solid Minerals

***[1]Teghware Orduvwe Alex, [2]Agbalagba Ogheneyerhovwo Ezekiel and [3]Avwiri Onomakere Gregory**

[1]Department of Physics, Federal University of Petroleum Resources, Effurun, Delta State, Nigeria.
[2]Department of Physics, Federal University of Petroleum Resources, Effurun, Delta State, Nigeria.
[3]Department of Physics, University of Port Harcourt, Rivers State, Nigeria.

*Corresponding author's email: teghware.alex@fupre.edu.ng

ABSTRACT

Natural radionuclides in solid minerals contribute to terrestrial radiation exposure, particularly where mining, processing, and industrial use increase human contact with naturally occurring radioactive materials. This study presents a multivariate statistical evaluation and comparative radiological risk ranking of K-40, U-238, and Th-232 in fifty selected solid mineral samples from Nigeria. Activity concentrations and radiological hazard parameters determined by gamma-ray spectrometry were evaluated using descriptive statistics, Pearson correlation, principal component analysis (PCA), hierarchical clustering, composite risk scoring, and Monte Carlo uncertainty analysis. Activity concentrations ranged from 108.36–223.37 Bq kg^{-1} for K-40, 9.07–16.72 Bq kg^{-1} for U-238, and 2.00–7.33 Bq kg^{-1} for Th-232. Positive correlations ($r > 0.996$) among the radionuclides indicate common geochemical controls and co-occurrence within mineral matrices. PCA revealed that a single component accounted for nearly all standardized variance, demonstrating that radiological behaviour is predominantly governed by a unified radioelement loading factor. Comparative risk ranking identified zircon sand, columbite, tin concentrate, phosphate, monazite, tantalite, zircon, granite, and wolframite as priority materials for monitoring. However, all radium equivalent activity values remained well below the 370 Bq kg^{-1} UNSCEAR limit, while external and internal hazard indices were below unity. Monte Carlo analysis showed narrow distributions for zircon sand, columbite, tin concentrate, phosphate, monazite, and tantalite, with mean values of approximately 41.4–44.4 Bq kg^{-1} and low standard deviations ($\sigma \approx 0.2–0.3$). Overall, the studied minerals are radiologically acceptable under normal use, although targeted monitoring is recommended during mining and processing, particularly during crushing, concentration, handling, storage, transportation, and industrial processing operationss.

Keywords:
Natural radioactivity,
Solid Minerals,
Radiological Hazard Indices,
Principal Component Analysis,
Hierarchical Clustering,
Monte-Carlo Uncertainty,
Risk Ranking,
Nigeria.

INTRODUCTION

Naturally occurring radioactive materials are intrinsic constituents of rocks, soils and mineral deposits (Agbalagba *et al.*, 2021). The most important primordial radionuclides for environmental gamma exposure are (^{40}K), (^{238}U), and (^{232}Th), together with the radiologically relevant daughters of the uranium and thorium decay series. Their concentrations in geological materials are controlled by lithology, mineralogy, weathering history, magmatic differentiation and sedimentary sorting (Paul *et al.*, 2022). In mineral-producing regions, these controls become important because mining, crushing, beneficiation and industrial utilization can increase occupational and public contact with radionuclide-bearing materials (Ademola *et al.*, 2014; Suleiman *et al.*, 2022)

Nigeria possesses diverse solid mineral resources hosted by basement complex rocks, younger granites, sedimentary basins and coastal plain formations (Michael & Peter, 2016). Materials such as granite, marble, limestone, gypsum, clay, coal, heavy mineral sands, rare-metal ores and industrial minerals are increasingly

exploited for construction, manufacturing and economic diversification. Although, Previous studies have reported natural radioactivity in soils, quarry environments, and localized mining settings in Nigeria (Ugbede & Echeweozo, 2017; Agbalagba et al., 2021; Ajetunmobi et al., 2022). For example, Ugbede and Echeweozo (2017) assessed background ionizing radiation and associated radiological risk parameters around a single quarry environment, whereas Ajetunmobi et al. (2022) investigated radionuclide activity concentrations and radiological indices in rock samples from a localized geological setting. Agbalagba et al. (2021) similarly examined radionuclide contamination and radiological risks in soils from selected mining sites. While these studies provide valuable site-specific evidence, relatively limited attention has been devoted to integrating radionuclide activity concentrations with multivariate statistical classification and comparative risk ranking across a broad suite of mineral commodities. This gap constrains the systematic identification of mineral groups requiring priority attention in routine radiological surveillance and risk-informed regulatory management.

The United Nations Scientific Committee on the Effects of Atomic Radiation (UNSCEAR, 2000; IAEA, 2018) recognizes mining as a major pathway for the redistribution of NORM and hazardous elements in the environment (Faanu et al., 2011). Globally, the radiological effects of exposure to ionizing radiation depend on the dose received and the duration of exposure. Health impacts may be somatic, affecting the exposed individual, or genetic, affecting future generations (Innocent *et al.,* 2013). Therefore, establishing baseline environmental data is necessary to support regulatory actions, improve occupational safety, and guide environmental protection strategies. This study aims to use multivariate statistical tools and a risk-ranking approach to provide regulators and mining operators with a broader view of which mineral to prioritize for radiological attention. The specific objectives are to: (i) summarize the distribution of K-40, U-238 and Th-232 across mineral classes; (ii) evaluate the correlation structure among radionuclides; (iii) determine the dominant multivariate components controlling the data; (iv) assess clustering tendencies among mineral samples; and (v) rank the samples according to relative radiological priority using a composite score derived from standard hazard indices, carry out probability uncertainty assessment using monte-carlo simulation.

MATERIALS AND METHODS

Study Area

Nigeria is located in West Africa between approximately latitudes 4°N–15°N and longitudes 3°E–14°E within the Pan-African mobile belt, situated between the West African and Congo Cratons. The country is divided into six geopolitical zones: North West, North East, North Central, South West, South South, and South East. Its geology comprises three major rock units: Precambrian Basement Complex rocks, sedimentary formations, and minor volcanic rocks. The Basement Complex, consisting mainly of granite, gneiss, and schist, hosts significant mineral resources such as gold, tin, and gemstones, particularly within the Jos Plateau. Sedimentary basins, including the Niger Delta and Benue Trough, contain petroleum, coal, limestone, barite, and other industrial minerals. The geological diversity of Nigeria reflects complex tectonic and depositional processes, which have influenced the distribution of mineral resources and shaped major landforms. These geological characteristics make Nigeria a suitable region for mineralogical, environmental, and radiological studies (Michael & Peter, 2016).

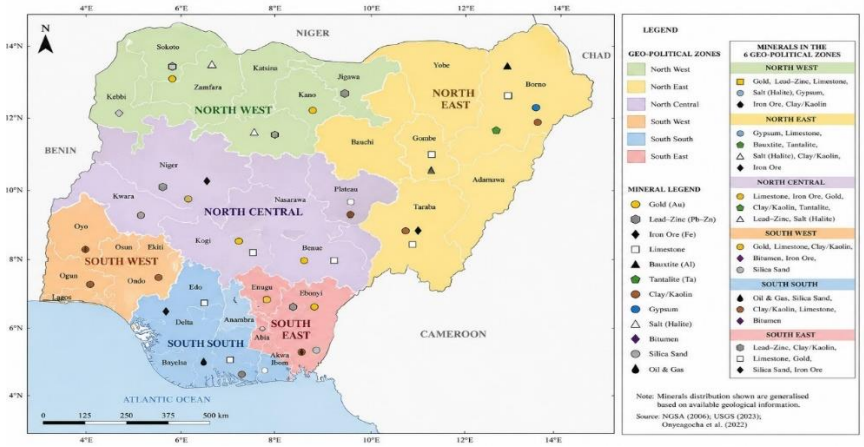

Figure 1: Map of Nigeria showing the geopolitical zones of the mineral samples (Paul et al., 2022)

Mineral Sampling Collection

In this study, Fifty (50) mineral samples were collected from different locations within the six geopolitical zones in Nigeria, capturing spatial variability in radionuclide distribution for the study with the help of the National Metallurgical Development Center. Jos, Plateau State, Nigeria. The collected mineral samples were sealed in a black polythene bag and carefully labeled with masking tape and pen/marker to avoid sample mix-up. The labelled mineral bags were then taken to the Lab for preparation before being transported to the National Institute of Radiation Protection and Research (NIRPR), Ibadan, Nigeria, for processing using NaI-TI gamma spectrometry measurements and analysis.

Mineral Sample Preparation

The mineral samples were sun-dried to constant weight to remove moisture content and prevent photon attenuation (Coker *et al.,* 2013). Dried samples were crushed using a mechanical crusher and an agate mortar. The pulverized samples were sieved to obtain homogeneous grain size distributions using a 500 µm mesh sieved. Prepared samples were sealed in airtight Marinelli beakers and stored for approximately 28 days to attain secular equilibrium between ^{226}Ra and its progeny (Godwin *et al.*, 2019; Okoye *et al.*, 2022) before being transported for analysis using the gamma ray spectrometry analyzer.

Dataset and Methodology

The dataset comprised fifty (50) selected solid mineral samples representing seven mineral-use classes: metallic minerals, industrial minerals, rock minerals, energy minerals, clay minerals, soil minerals and sedimentary minerals. The samples covered commercially relevant materials such as zircon sand, columbite, tin concentrate, monazite, tantalite, wolframite, granite, phosphate, laterite, gypsum, coal, kaolin, limestone, glass sand and related materials. This classification permits comparison between ore-associated minerals, rock-forming materials and low-activity sedimentary or clay-rich samples. For each sample, the activity concentrations of (^{238}U, ^{232}Th, and ^{40}K)) were used together with derived radiological hazard indices to evaluate the comparative risking.

Absorbed Dose Rate (D)

The absorbed dose rate represents the gamma radiation dose delivered in air at 1 m above ground level and is expressed in nGy h^{-1} (Agbalagba *et al.*, 2012; Ajeh *et al.*, 2022).

$$D_R = 0.462C_U + 0.604C_{Th} + 0.0417C_K \quad (1)$$

Radium Equivalent Activity (Raeq)

Raeq provides a unified radiological index representing combined activities of (^{40}K), (^{238}U), and (^{232}Th) (Avwiri *et al.,* 2017; Alausa *et al.*, 2025).

$$Ra_{eq} = C_U + 1.43C_{Th} + 0.077C_K \quad (2)$$

Annual Effective Dose Equivalent (AEDE)

AEDE estimates annual human exposure considering occupancy factors and dose conversion coefficients (Ononugbo *et al.*, 2017; Nduka *et al.*, 2022).

$$\text{AEDE (outdoor)} = (D_R) \text{ x } 8760 \text{ x } (0.7 \text{ x } 10^{-3}) \quad (3)$$

External Hazard Index (Hex)

Hex evaluates external gamma exposure hazards from radionuclide-containing materials (Agbalagba *et al.*, 2021; UNSCEAR 2000)

$$(H_{ex}) = C_U/370 + C_{Th}/259 + C_K/4810 \quad (4)$$

Internal Hazard Index (Hin)

Hin accounts for internal exposure risks, especially from radon inhalation (Agbalagba *et al.*, 2021; UNSCEAR, 2000).

$$(H_{in}) = C_U/185 + C_{Th}/259 + C_K/4810 \quad (5)$$

Excess Lifetime Cancer Risk (ELCR)

ELCR estimates the probability of developing cancer over a lifetime due to prolonged radiation exposure (Dembo *et al.*, 2023; Echeweozo *et al.*, 2024).

$$\text{ELCR} = (AEDE) \text{ x DL x RF} \quad (6)$$

The indices considered in the multivariate risk-ranking procedure included radium equivalent activity, absorbed dose rate, annual effective dose equivalent, external hazard index, internal hazard index, representative gamma index, alpha index and excess lifetime cancer risk.

Comparative Risk Ranking

To generate a relative risk ranking, ten radiological hazard indices variables were used (Raeq, Dose-rate (D), outdoor AEDE, indoor AEDE, Hex, Hin, Iγ, Iα, outdoor ELCR, and indoor ELCR). Since the selected radiological parameters have different units and magnitudes, (min-max) normalization was applied before aggregation (Nardo et al., 2008). The normalized value of each radiological parameter was obtained (UNSCEAR, 2000; OECD/NEA, 1979)

$$Z_{ij} = \frac{(X_{ij} - X_{ijmin})}{(X_{jmax} - X_{jmin})} \quad (7)$$

Where Z_{ij} is the normalized value of the jth radiological parameter for the ith mineral sample, X_{ij} is the original value of the parameter (Raeq, Dose-rate (D), outdoor AEDE, indoor AEDE, Hex, Hin, Iγ, Iα, outdoor ELCR,

and indoor ELCR), X_{jmin} is the minimum value of the parameter among all samples, and X_{jmax} is the maximum value of the same parameter among all samples. The composite risk score, therefore, becomes;

$$CRS_i = \left(\frac{100}{m}\right) x \sum Z_{ij} \quad (8)$$

Where CRS_i is the composite risk score of the ith mineral sample, (m) is the number of radiological parameters included in the ranking, and $\sum Z_{ij}$ is the sum of the normalized values of the selected radiological parameters. The normalized values were averaged and multiplied by 100 to obtain a composite relative risk score. A higher CRS value indicates a higher relative radiological priority among the investigated solid minerals. The resulting scores were divided into four quartile-based relative tiers: low risk, moderate risk, high risk and very high risk. The term "very high risk" in this classification refers only to relative ranking within the investigated dataset and does not necessarily indicate that a mineral sample exceeds internationally recommended radiological safety limits (Nardo et al., 2008)

Multivariate statistical treatment

Descriptive statistics were computed by mineral class. Pearson correlation analysis was used to evaluate pairwise associations among K-40, U-238 and Th-232. Principal component analysis was then applied to standardized radionuclide variables to reduce dimensionality and identify the dominant latent factor controlling natural radioactivity. The standardized dataset of radionuclide activity concentrations (^{238}U, ^{232}Th, ^{40}K) was decomposed into principal components:

$$Z = XW \quad (9)$$

Where X is the standardized data matrix, W the eigenvector matrix of the covariance matrix C, and Z the principal component scores. Eigenvalues (λ) and eigenvectors (v) were obtained from:

$$Cv = \lambda v \quad (10)$$

Principal component analysis (PCA) was applied to the standard (^{40}K, ^{238}U, and ^{232}Th) activity concentrations to identify the dominant latent structure underlying radionuclide variability. Hierarchical clustering was performed using Ward linkage on standardized radionuclide concentrations to explore whether the samples naturally separated according to mineral class or geological affinity. Uncertainty in radiological hazard indices was quantified using Monte Carlo simulations with 10,000 iterations per mineral sample, implemented in Python. A one-way analysis of variance was additionally applied to compare selected response variables across mineral classes. The ANOVA results are interpreted cautiously because some classes contained small numbers of samples, especially the sedimentary, energy and rock categories. Consequently, ANOVA was used as a screening tool rather than as the sole basis for inference.

RESULTS AND DISCUSSION

Descriptive Distribution of Radionuclides and Radiological Hazards by Mineral Class

Table (1 – 7) shows the mineral class specific activity concentration based on their mineral class characterization.

Table 1: Specific Activity Concentration of (^{40}K, ^{238}U, and ^{232}Th (Bq Kg-1) Results of Metallic Minerals

S/N	Minerals	K-40 (Bq/kg)	U-238 (Bq/kg)	Th-232 (Bq/kg)
1.	Magnetite	164.34±1.55	12.79±0.12	4.43±0.08
2.	Iron Ore	167.62±1.57	13.01±0.12	4.57±0.08
3.	Tin Concentrate	214.86±1.81	16.15±0.14	7.08±0.10
4.	Columbite	220.19±1.83	16.51±0.14	7.23±0.10
5.	Bismuth	127.29±1.33	10.33±0.11	3.08±0.06
6.	Manganese	157.84±1.51	12.36±0.12	4.07±0.07
7.	Lithium	128.97±1.34	10.44±0.11	2.95±0.06
8.	Molybdenite	133.48±1.37	10.74±0.11	3.16±0.07
9.	Tantalite	209.41±1.78	15.79±0.13	6.62±0.10
10.	Zinc	175.71±1.61	13.55±0.12	5.30±0.09
11.	Lead	168.14±1.57	13.05±0.12	4.68±0.08
12.	Wolframite	203.71±1.75	15.41±0.13	6.28±0.09
13.	Iron	131.33±1.36	10.60±0.11	2.96±0.06
MEAN VALUE		169.45±1.56	13.13±0.12	4.80±0.07

Table 2: Specific Activity Concentration of (^{40}K, ^{238}U and ^{232}Th (Bqkg^{-1}) Results of Industrial Solid Minerals

S/N	Minerals	K-40 (Bq/kg)	U-238 (Bq/kg)	Th-232 (Bq/kg)
1.	Gypsum	129.75±1.35	10.49±0.11	3.09±0.06
2.	Magnesite	110.00±1.22	9.18±0.100	2.0±0.050
3.	Glass Sand	134.06±1.37	10.78±0.11	3.0±0.060
4.	Rutile	177.90±1.62	13.07±0.12	5.32±0.09
5.	Silica Sand	113.60±1.24	9.42±0.020	2.08±0.05
6.	Sepiolite	139.30±1.40	11.13±0.11	3.31±0.07
7.	Bentonite	163.27±1.54	12.72±0.12	4.57±0.08
8.	Zircon Sand	223.37±1.85	16.72±0.14	7.33±0.10
9.	Limestone	124.58±1.31	10.15±0.11	2.67±0.06
10.	Phosphate	214.24±1.80	16.11±0.14	6.95±0.11
11.	Mica	155.30±1.50	12.19±0.12	4.1±0.080
12.	Phosphate Clay	189.23±1.68	14.45±0.13	5.85±0.09
13.	Monazite	213.75±1.80	16.08±0.14	6.92±0.10
14.	Feldspar	157.08±1.51	12.31±0.12	4.15±0.08
15.	Kyanite	143.50±1.43	11.41±0.11	3.83±0.07
16.	Ilmenite	199.50±1.73	15.13±0.13	6.34±0.09
17.	Baryte	175.92±1.61	13.56±0.12	5.01±0.08
18.	Zircon	206.49±1.77	15.6±0.13	6.37±0.09
19.	Fluorite	165.89±1.56	12.9±0.12	4.50±0.08
20.	Diatomite	108.36±1.21	9.07±0.11	2.02±0.05
21.	Graphite	156.61±1.51	12.28±0.12	4.07±0.07
22.	Ilmenite (alt)	191.32±1.69	14.59±0.13	5.83±0.09
MEAN VALUE		**163.32±1.65**	**12.70±0.13**	**4.51±0.08**

Table 3: Specific Activity Concentration of (^{40}k, ^{238}u, and ^{232}th (Bqkg^{-1}) Results of Clay Minerals

S/N	Minerals	K-40 (Bq/kg)	U-238 (Bq/kg)	Th-232 (Bq/kg)
1.	Fire Clay	112.14±1.23	9.32±0.10	2.16±0.05
2.	Smectite	132.33±1.36	10.66±0.11	2.99±0.06
3.	Ball Clay	119.67±1.28	9.82±0.11	2.62±0.06
4.	Kaolin	159.96±1.52	12.50±0.12	4.53±0.08
5.	Halloysite	135.97±1.38	10.91±0.11	3.25±0.07
MEAN VALUE		132.01±1.35	10.64±0.11	3.11±0.07

Table 4: Specific Activity Concentration of (^{40}K, ^{238}U and ^{232}Th (Bqkg^{-1}) Results of Soil/Clay Minerals

S/N	Minerals	K-40 (Bq/kg)	U-238 (Bq/kg)	Th-232 (Bq/kg)
1.	Laterite	170.03±1.58	13.17±0.12	5.04±0.08
2.	Silty Clay	121.71±1.30	9.96±0.11	2.54±0.06
3.	Clay	120.57±1.29	9.88±0.11	2.49±0.06
4.	Sandy Clay	114.82±1.25	9.50±0.10	2.12±0.05
5	Loamy Clay	136.96±1.39	10.97±0.11	3.54±0.07
MEAN VALUE		132.82±1.39	10.20±0.11	3.15±0.07

Table 5: Specific Activity Concentration of (^{40}K, ^{238}U, and ^{232}Th (Bqkg^{-1}) Results of Energy Minerals.

S/N	Minerals	K-40 (Bq/kg)	U-238 (Bq/kg)	Th-232 (Bq/kg)
1.	Bituminous Sand	132.72±1.36	10.69±0.11	3.12±0.07
2.	Coal	159.82±1.52	12.49±0.12	4.44±0.08
MEAN VALUE		146.27±1.44	11.59±0.12	3.78±0.07

Table 6: Specific Activity Concentration of (^{40}K, ^{238}U and ^{232}Th (Bqkg^{-1}) Results of Rock Minerals

S/N	Minerals	K-40 (Bq/kg)	U-238 (Bq/kg)	Th-232 (Bq/kg)
1.	Granite	205.29±1.76	15.52±0.13	6.37±0.09
2.	Marble	128.46±1.34	10.41±0.11	2.82±0.06
MEAN VALUE		166.86±1.55	12.97±0.12	4.60±0.07

Table 7: Specific Activity Concentration of (^{40}K, ^{238}U and ^{232}Th (Bqkg^{-1}) Results of Sedimentary Minerals

S/N	Minerals	K-40 (Bq/kg)	U-238 (Bq/kg)	Th-232 (Bq/kg)
1.	Shale	126.09±1.32	10.25±0.11	2.66±0.06
MEAN VALUE		126.09±1.32	10.25±0.11	2.66±0.06

The complete dataset comprised 50 mineral samples. Across all samples, K-40 ranged from 108.36 to 223.37 Bq kg^{-1}, U-238 ranged from 9.07 to 16.72 Bq kg^{-1} and Th-232 ranged from 2.00 to 7.33 Bq kg^{-1}. These ranges indicate moderate natural variability but no extreme radionuclide enrichment within the investigated mineral suite.

Metallic and rock minerals recorded the highest mean radionuclide levels, reflecting the influence of crystalline and ore-associated geological settings (Ademola et al., 2014). Industrial minerals also showed elevated values where heavy-mineral or phosphate-bearing materials were present. Soil/clay and sedimentary minerals generally recorded lower activity concentrations, consistent with dilution, weathering, and redistribution of uranium- and thorium-bearing accessory minerals (Aliyu *et al.*, 2015). Figure 2 illustrates the same class-level pattern. K-40 dominates the activity concentration scale in every class, whereas U-238 and Th-232 occur at lower absolute concentrations. For visual comparability, U-238 and Th-232 are multiplied by a factor of ten in the figure. From Table 9, the low radiological hazard indices observed across all samples suggest minimal external and internal radiation exposure risks to workers and the general public. The computed absorbed dose rates and annual effective dose equivalents were substantially below internationally recommended exposure limits, indicating that prolonged utilization of these materials is unlikely to produce significant radiological health effects.

Table 8: Mineral-Class Distribution and Mean Radionuclide/Radium Equivalent Values

Class	N	K-40 mean±SD	U-238 mean±SD	Th-232 mean±SD	Raeq mean±SD
Metallic	13	169.45 ± 33.88	13.13 ± 2.25	4.80 ± 1.58	33.05 ± 7.12
Industrial	22	163.32 ± 35.65	12.70 ± 2.36	4.51 ± 1.68	31.73 ± 7.51
Rock	2	166.88 ± 54.33	12.96 ± 3.61	4.59 ± 2.51	32.38 ± 11.39
Energy	2	146.27 ± 19.16	11.59 ± 1.27	3.78 ± 0.93	28.26 ± 4.08
Clay	5	132.01±1.35	10.64±0.11	3.11±0.07	132.01±1.35
Soil/Clay	5	132.82±1.39	10.20±0.11	3.15±0.07	132.82±1.39
Sedimentary	1	126.09± 18.20	10.25± 1.13	2.66± 0.24	23.76± 3.79
Mean	50	148.12±20.76	11.64±2.52	3.84±0.92	25.35±3.46

Table 9: Mean Values of the Radiological Parameter for All Solid Minerals Compared with World Permissible Limits *(UNSCEAR, IAEA, and E.U Guidelines)*

Class	n	D (nGyh^{-1})	AEDE Outdoor (mSvy^{-1})	AEDE Indoor (mSvy^{-1})	H_{ex} (mSvy^{-1})	H_{in} (mSvy^{-1})	Iγ	Iα	ELCR Outdoor (×10^{-3})	ELCR Indoor (×10^{-3})
Metallic	13	16.033	0.020	0.079	0.089	0.125	0.248	0.066	0.069	0.275
Industrial	22	15.403	0.019	0.076	0.086	0.120	0.239	0.064	0.066	0.264
Rock	2	15.724	0.020	0.077	0.088	0.123	0.244	0.065	0.068	0.270
Energy	2	13.738	0.017	0.068	0.077	0.108	0.213	0.058	0.059	0.236
Clay	5	12.300	0.015	0.060	0.068	0.097	0.190	0.053	0.053	0.211
Soil/clay	5	12.380	0.015	0.061	0.069	0.097	0.191	0.054	0.053	0.213
Sedimentary	1	11.600	0.014	0.057	0.064	0.092	0.179	0.051	0.050	0.199
Mean	50	13.883	0.017	0.068	0.077	0.109	0.215	0.059	0.060	0.238

Class	n	D ($nGyh^{-1}$)	AEDE Outdoor ($mSvy^{-1}$)	AEDE Indoor ($mSvy^{-1}$)	H_{ex} ($mSvy^{-1}$)	H_{in} ($mSvy^{-1}$)	Iγ	Iα	ELCR Outdoor ($\times10^{-3}$)	ELCR Indoor ($\times10^{-3}$)
WORLD PERMISSIBLE LIMITS		59	0.070	0.410	1.0	1.0	1.0	1.0	0.29	1.16

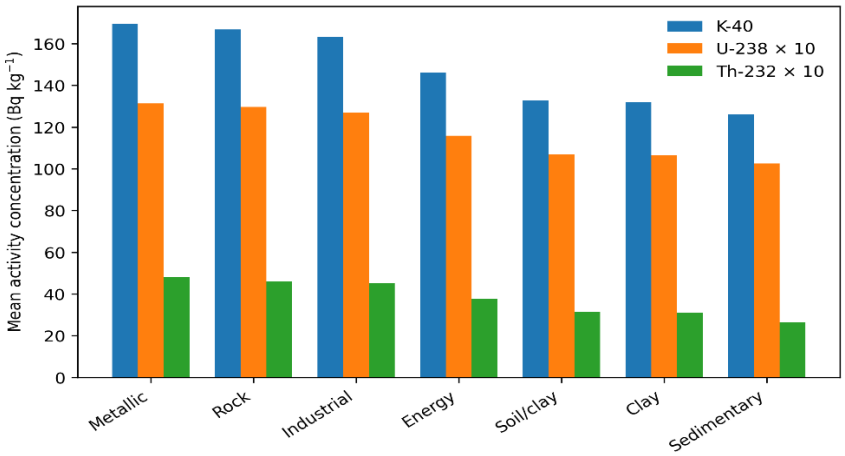

Figure 2: Mean activity concentrations by mineral class. ^{238}U and ^{232}Th are plotted as tenfold values to improve visual comparability with ^{40}K

Correlation Structure among (^{238}U, ^{232}Th, and ^{40}K).
The Pearson correlation matrix shows very strong positive relationships among the three radionuclides. The correlation coefficient between K-40 and U-238 was approximately 0.999, between K-40 and Th-232 approximately 0.997 and between U-238 and Th-232 approximately 0.996. These near-collinear relationships demonstrate that the radionuclides are controlled by a shared radioelement loading structure rather than independent processes.

Geochemically, this pattern is reasonable. Uranium and thorium are commonly enriched in accessory minerals such as zircon, monazite and other heavy-mineral phases, whereas K-40 is linked to potassium-bearing silicates. In the present dataset, samples with higher K-40 also tended to show higher U-238 and Th-232, suggesting that the highest relative risks are associated with broader mineralogical enrichment rather than isolated elevation of only one radionuclide.

Table 10: Pearson Correlation Matrix for Radionuclide Activity Concentrations

Radionuclide	^{40}K	^{238}U	^{232}Th
^{40}K	1.000000	0.999247	0.997163
^{238}U	0.999247	1.000000	0.996000
^{232}Th	0.997163	0.996000	1.000000

Principal Component Interpretations
PCA of the mineral samples are interpreted primarily as a confirmatory assessment of the common variance structure rather than as a substantial dimensionality reduction procedure. It confirms a strong correlation structure between radionuclides. PC1 explained 99.83% of the standardized variance, while PC2 contributed approximately 0.17%. This indicates that the dataset can be represented mainly by a single latent factor, here interpreted as a general radioelement loading factor. The positive loadings of K-40, U-238 and Th-232 on PC1 show that samples with high PC1 scores are simultaneously enriched in the three radionuclides.
From Figure 3, the small contribution of PC2 suggests that differential enrichment among the radionuclides is minor compared with the shared variance. Therefore, multivariate reduction does not reveal separate independent uranium-, thorium-, or potassium-dominated populations; instead, the samples form a continuous gradient from low to high radioactivity.

Table 11: PCA Loadings for Standardized Radionuclide Variables

Variable	PC1	PC2	Explained variance (%)
^{40}K	1.0098	-0.0184	PC1 = 99.83; PC2 = 0.17
^{238}U	1.0094	-0.0355	
^{232}Th	1.0087	0.0540	

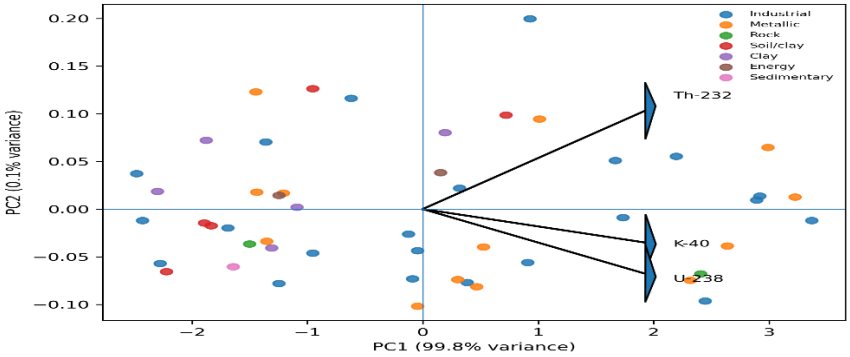

Figure 3: PCA biplot of standardized radionuclide concentrations. Sample scores are colored by mineral class; arrows represent variable loadings

Hierarchical Clustering and Class Separation

Hierarchical clustering from figure 4 showed gradual linkage rather than sharply separated natural groups. This supports the PCA interpretation that the dataset is structured along a continuous radioactivity gradient. Although ore-associated and heavy-mineral samples tended to occupy the higher loading side of the data structure, clustering was not determined solely by the broad mineral-use class.

This finding is important for regulatory interpretation. Broad labels such as industrial mineral, metallic mineral or clay mineral are useful for description, but they cannot replace sample-specific radiological measurement. Some industrial minerals, such as zircon sand, phosphate, monazite and ilmenite, had higher relative scores than several metallic samples. Conversely, some metallic materials, including bismuth, lithium, molybdenite and iron, were positioned within lower tiers.

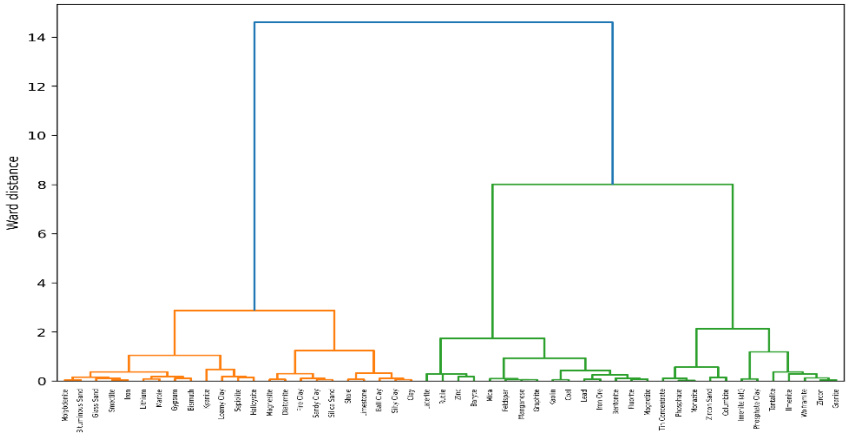

Figure 4: Hierarchical clustering dendrogram based on standardized K-40, U-238 and Th-232 activity concentrations using Ward linkage

Comparative Risk Ranking

The composite ranking from figure 5 identified zircon sand as the highest relative-priority sample, with Ra-eq = 44.401 Bq kg^{-1} and a composite score of 100.00. Other high-ranking samples included columbite, tin concentrate, phosphate, monazite, tantalite, zircon, granite, wolframite, ilmenite and phosphate clay. These samples are associated mainly with heavy-mineral sands, rare-metal ores, phosphate-bearing materials and crystalline rock matrices.

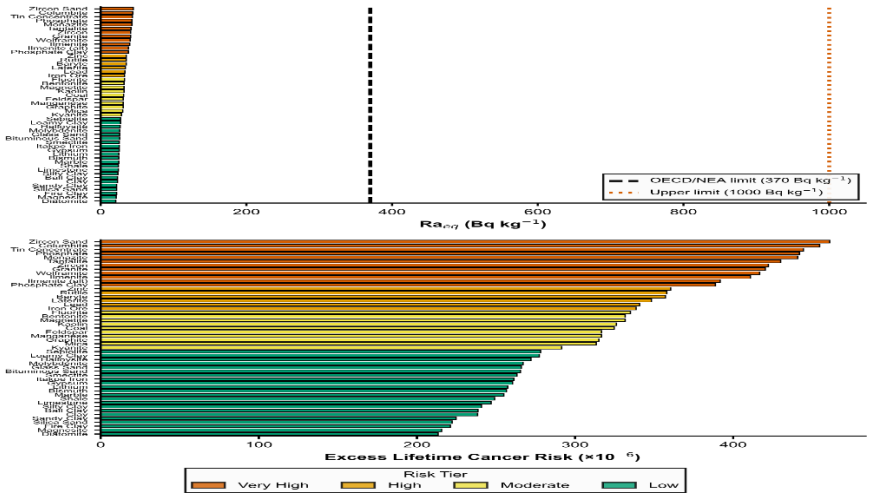

Figure 5: Radiological risk ranking of the selected solid minerals understudy: (a) Radium equivalent activity and (b) Excess lifetime cancer risk. Colors indicate risk tiers based on composite scoring for each sample

Despite their relative priority, all samples were far below the Ra_eq screening level of 370 Bq kg^{-1}. The maximum Ra_eq was 44.401 Bq kg^{-1}, representing only about 12.0% of the screening criterion. Similarly, the highest values of H_ex (0.120), H_in (0.165) and I gamma (0.334) were below unity. The implication of this risk score is that priority should be given to minerals likely to generate radioactive dust or be stockpiled in large quantities, even where absolute dose criteria are not exceeded. Table 12 shows the top ten composite relative radiological risk score of minerals that falls into the very high quartile-based tiers of the entire mineral samples.

Table 12: Top Ten Samples in the Comparative Relative Risk Ranking

Rank	Mineral	Class	Raeq	Dose rate	Hex	Hin	Ig	ELCR outdoor x10-3	Composite score	Relative risk tier
1	Zircon Sand	Industrial	44.401	21.466	0.120	0.165	0.334	0.092	100.000	Very high (relative)
2	Columbite	Metallic	43.804	21.176	0.118	0.163	0.329	0.091	97.794	Very high (relative)
3	Tin Concentrate	Metallic	42.819	20.697	0.116	0.159	0.322	0.089	93.366	Very high (relative)
4	Phosphate	Industrial	42.545	20.574	0.115	0.158	0.320	0.088	92.282	Very high (relative)
5	Monazite	Industrial	42.434	20.522	0.115	0.158	0.319	0.088	91.829	Very high (relative)
6	Tantalite	Metallic	41.381	20.026	0.112	0.154	0.311	0.086	87.991	Very high (relative)
7	Zircon	Industrial	40.609	19.665	0.110	0.152	0.305	0.084	84.449	Very high (relative)
8	Granite	Rock	40.436	19.578	0.109	0.151	0.304	0.084	83.875	Very high (relative)
9	Wolframite	Metallic	40.076	19.407	0.108	0.150	0.301	0.083	82.352	Very high (relative)
10	Ilmenite	Industrial	39.558	19.139	0.107	0.148	0.297	0.082	79.743	Very high (relative)

Monte-Carlo Uncertainty Analysis

The multi-panel probability density distributions of radium equivalent activity (Raeq) for the investigated mineral assemblages provide a statistically robust analysis for evaluating radiological safety and lithological variability. Across all six mineral types, zircon sand, columbite, tin concentrate, phosphate, monazite, and tantalite, which are characterized by relatively high activity concentration values, exhibit remarkably narrow distributions, with mean values constrained within the range of approximately (41.4–44.4) Bq/kg. The corresponding standard deviations ($\sigma \approx$ 0.2–0.3) indicate minimal dispersion, reflecting high analytical precision and limited heterogeneity within each mineral class. This degree of clustering suggests that the radionuclide contributions from (^{238}U, ^{40}K, and ^{232}Th)

is consistently low and exhibit negligible stochastic variability under the applied Monte Carlo simulation.

The figure 6 provides compelling probabilistic evidence that all investigated mineral type's exhibit low and statistically stable Raeq values, with negligible radiological risk. The clear separation from the safety threshold, combined with narrow uncertainty bounds, supports the conclusion that these materials are radiologically benign and suitable for both industrial utilization and environmental exposure scenarios without the need for additional radiological control measures.

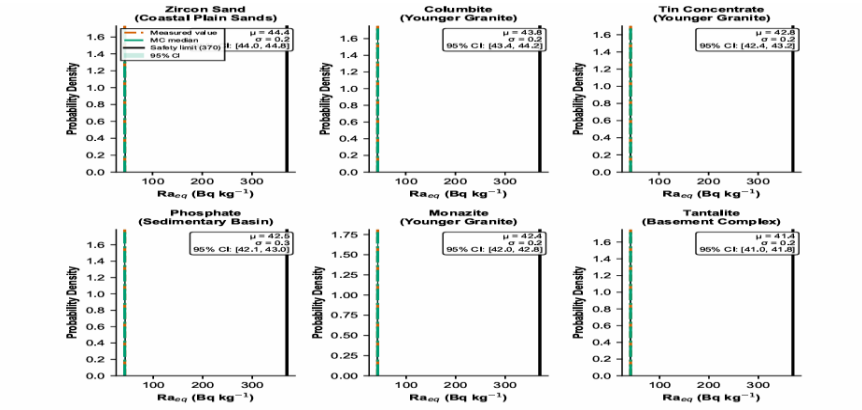

Figure 6: Monte Carlo uncertainty distributions for the six highest-risk mineral samples. Histograms show 10,000 simulations with measured values, MC medians, and 95% confidence intervals

Environmental and Regulatory Implications

The findings indicate that the studied minerals are radiologically acceptable under normal handling and use conditions. However, the purpose of multivariate ranking is to improve decision-making under realistic mining and industrial scenarios. Minerals in the highest relative tiers may still require closer attention because workers can experience repeated exposure through inhalation of fine dust, direct handling of concentrates, equipment contamination and prolonged storage of bulk materials.

A regulatory approach based only on broad regional or mineral class labels may miss localized enrichment. The evidence supports a tiered monitoring framework in which high-priority samples undergo more frequent gamma spectrometric screening and workplace dose assessment, while low-priority materials are monitored at longer intervals. Such a framework would make radiological surveillance more efficient without imposing unnecessary restrictions on minerals that are clearly below international hazard thresholds.

CONCLUSION

This study presented a focused multivariate statistical evaluation and comparative risk ranking of natural radionuclides in fifty Nigerian solid mineral samples.^{238}U, ^{232}Th, and ^{40}Kwere present in all mineral classes, but their activity concentrations were below international reference values. Strong positive correlations among the radionuclides and a dominant first principal component demonstrate that the dataset is governed mainly by a common radioelement loading factor. Hierarchical clustering revealed a continuous radiological gradient rather than sharply separated mineral groups.

The composite ranking identified heavy-mineral and ore-associated samples, particularly zircon sand, columbite, tin concentrate, phosphate, monazite, tantalite, zircon, granite, wolframite, ilmenite and phosphate clay, as the highest relative-priority materials for monitoring. Monte Carlo uncertainty approach which evaluates uncertainty in the highest-ranked mineral shows that Zircon sand with a mean value of 44.40 has zero probability of exceeding the 370Bq/Kg screening threshold limits. Nevertheless, all evaluated hazard indices were below international screening limits, including Ra_eq < 370 Bq kg^{-1} and other hazard indices below unity. The results therefore support the safe use of the studied minerals for construction, manufacturing and other economic diversity purposes, while recommending targeted radiological monitoring in mining, processing and storage environments where dust generation and prolonged occupational exposure may occur

REFERENCES

Ademola, A. K., Bello, A. K., & Adejumobi, A. C. (2014). Determination of natural radioactivity and hazard

in soil samples in and around gold mining area in Itagunmodi, south-western Nigeria. *Journal of Radiation Research and Applied Sciences*, *7*(3), 249–255. https://doi.org/10.1016/j.jrras.2014.06.001.

Agbalagba, E. O., Avwiri, G. O., & Chad-Umoreh, Y. E. (2012). Γ-Spectroscopy measurement of natural radioactivity and assessment of radiation hazard indices in soil samples from oil fields environment of Delta State, Nigeria. *Journal of Environmental Radioactivity*, *109*, 64–70. https://doi.org/10.1016/j.jenvrad.2011.10.012.

Ajeh, E. A., Yusuf, N., & Garba, N. N. (2022). Radiological characterization of radioactive minerals associated with tin mining activities in Nigeria. *Environmental Monitoring and Assessment*, 194(7), 501–514. https://doi.org/10.9734/ajopacs/2023/v11i3203

Ajetunmobi, A. E., Biere, P., Alausa, S. K., Coker, J. O., David, T. W., Talabi, A. T., Oladujoye, H. T., & Olojede, S. K. (2022). Measurement of activity concentrations of rock samples from rocks-surrounded town in Igbeti, Oyo State, Nigeria. *Scientia Africana*, *21*(1), 183–194. https://doi.org/10.4314/sa.v21i1.16.

Alausa, S. K., Ibrahim, A. K., & Bello, M. T. (2025). Radiological impact assessment of mine residues from coal mining sites at Awulu-Ika, Kogi State, Nigeria. *Environmental Earth Sciences*, 84(3), 115–128. *https://doi.org/10.4038/jur.v13i1.8053*

Aliyu, A. S., Ibrahim. U, Akpa, C. T., Garba, N. N., and Ramli, A. T. (2015). Assessment of naturally occurring radioactive materials in mining environments. *Environmental Earth Sciences*, 74(2), 1451–1460.

Avwiri, G. O., Agbalagba, E. O., & Ononugbo, C. P. (2017). Radioactive pollution and excess lifetime cancer risk due to gamma exposure of soil and groundwater around open landfills in Rivers State, Nigeria. Canadian Journal of Pure and Applied Sciences, 11(1), 4121-4130.

Coker, J. O., Mustapha, A. O., Makinde, V., & Adesodun, J. K. (2013). Application of radiometric surveys to delineate between sedimentary terrain and basement complex: A case study of Sagamu and Abeokuta, Southwestern Nigeria. Journal of Natural Sciences Research, 3(13), 34-42.

Dembo, T. S., Edori, O. S., & Edori, E. S. (2023). Radiological hazard assessment of asphalt plant environments in Delta State, Nigeria. *Radiation Protection and Environment*, 46(1), 34–45. https://dx.doi.org/10.56201/rjpst.v6.no2.2023.pg56.80

Echeweozo, E. O., Ugbede, F. O., & Agbalagba, E. O. (2024). Radioactivity concentration in soil and rock and their radiological implications to human health in Ugwuele quarry mining site, Uturu, Abia State, Nigeria. *Journal of Environmental Radioactivity*, 271, 107405. https://doi.org/10.4314/jasem.v28i2.31

Ekeocha, N. E. (2016). Radioactivity characterization of pyrochlore and xenotime minerals associated with tin mining in Jos Plateau, Nigeria. *Nigerian Journal of Science and Environment*, 14(2), 99–108.

Faanu, A., Ephraim, J. H., & Darko, E. O. (2011). Assessment of public exposure to naturally occurring radioactive materials from mining and mineral processing activities of Tarkwa Goldmine in Ghana. Environmental Monitoring Assessment, (180), 15–29.

Godwin H.A, Ferodous, J.J., Rahman, M.M., Rubina, R., Hasan, S. & Ferdous, N. (2019). Radioactivity Distributions in soils from Habiganj District, Bangladesh and their Radiological Implications. *Malaysian Journal of Soil Science*, **19**, 59 – 71.

IAEA. (2018). Radiation protection and safety of radiation sources: International basic safety standards. General Safety Requirements Part 3. International Atomic Energy Agency.

Innocent, A. J., Ibrahim, U., & Adamu, M. (2013). Assessment of natural radioactivity levels in mining environments in Northern Nigeria. *Journal of Environmental Physics*, 5(2),21-29.

Michael & Adeyeye, (2016). Profiling Nigeria's solid mineral sector: Challenges and prospects. *International Journal of Mining Science and Technology*, 26(2), 221–229. https://doi.org/10.1016/j.hazadv.2023.100288

Nduka, J.K., Umeh, T.C., Kelle, H.I., Ozoagu, P.C. & Okafor, P.C. (2022). Health risk assessment of radiation dose of background radionuclides in quarry soil and uptake by plants in Ezillo-Ishiagu in Ebonyi South-Eastern Nigeria. *Case Studies in Chemical and Environmental Engineering*, **6**, 15 - 24. https://doi.org/10.1016/j.cscee.2022.100269

Nardo, M., Saisana, M., Saltelli, A., Tarantola, S., Hoffmann, A., & Giovannini, E. (2008). *Handbook on constructing composite indicators: Methodology and user guide*. OECD Publishing. https://doi.org/10.1787/9789264043466-en.

OECD/NEA. (1979). Exposure to radiation from natural radioactivity in building materials. Organisation for

Economic Co-operation and Development/Nuclear Energy Agency.

Okoye, E.A., Ezejiofor, A.N., Nwaogazie, I.L. Frazzoli, C. & Orisakwe, O.E. (2022). Heavy metals and arsenic in soil and vegetation of Niger Delta, Nigeria: Ecological risk assessment. *Case Studies in Chemical and Environmental Engineering*, **6**, 1 – 8. https://doi.org/10.1016/j.cscee.2022.100222

Ononugbo, C. P., Avwiri, G. O., and Agbalagba, E. O. (2017). Radioactivity pollution and 41 excess lifetime cancer risk due to gamma exposure of soil and ground water around 42 open landfills in Rivers State, Nigeria. *Canadian Journal of Pure and Applied 43 Sciences* **11**(1), 4121-4130. https://doi.org/10.9734/ncjpas/2023/v11i3203

Paul, S. N., Frazzoli, C., Sikoki, F. D., Babatunde, B. B., & Orisakwe, O. E. (2022). Natural occurring radioactive materials (NORMs) from mining sites in Nigeria: A systematic review of geographical distribution and public health concern. *Journal of Environmental Radioactivity, 249*, 106889. https://doi.org/10.1016/j.jenvrad.2022.106889

Suleiman, A. B., Hassan, A. M., & Ibrahim, M. (2022). Evaluation of radiological hazards associated with selected mining sites in Niger State, Nigeria. *Journal of Radiation and Nuclear Applications*, 7(2), 89–101. https://doi.org/10.3126/hp.njrna.30001

Ugbede, F. O. (2020). Assessment of environmental radioactivity and associated radiological hazards in mining environments in Nigeria. *Journal of Radiation Research and Applied Sciences*, 13(2), 352–362.

UNSCEAR. (2000). Sources and effects of ionizing radiation. United Nations Scientific Committee on the Effects of Atomic Radiation, United Nations, New York.